Crystal Structure of Dimeric Heme Oxygenase-2 from *Synechocystis* sp. PCC 6803 in Complex with Heme[†,‡]

Masakazu Sugishima,[§] Yoshinori Hagiwara,[§] Xuhong Zhang,[||] Tadashi Yoshida,[||] Catharina T. Migita,[⊥] and Keiichi Fukuyama*[,§]

Department of Biology, Graduate School of Science, Osaka University, Toyonaka, Osaka 560-0043, Japan, Department of Biochemistry, Yamagata University School of Medicine, Yamagata 990-9585, Japan, Department of Biological Chemistry, Faculty of Agriculture, Yamaguchi University, 1677-1 Yoshida, Yamaguchi 753-8575, Japan

Received September 10, 2004; Revised Manuscript Received January 10, 2005

ABSTRACT: Phycobiliproteins, light-harvesting proteins in cyanobacteria, red algae, and cryptophytes, contain phycobilin pigments. Phycobilins are synthesized from biliverdin, which is produced by the oxidative cleavage of the heme porphyrin ring catalyzed by heme oxygenase (HO). Two paralogs of *ho* (*ho1* and *ho2*) have been identified in the genome of the cyanobacterium, *Synechocystis* sp. PCC 6803. The recombinant proteins of both paralogs (Syn HO-1 and Syn HO-2) possess *in vitro* heme degradation activity. We have determined the crystal structures of Syn HO-2 in complex with heme (heme-Syn HO-2) and its reduced and NO bound forms. The heme-Syn HO-2 crystal was a nonmerohedral twin, and detwinned diffraction data were used to refine the structure. Although heme-Syn HO-2 shares common folding with other HOs, the C-terminal segment is ordered and turns back to the heme-binding side. Gel-filtration chromatography analysis and molecular packing in the crystal indicate that heme-Syn HO-2 forms a homodimer, in which the C-terminal ordered segments interact with each other. Because Syn HO-2 is a monomer in the apo state, the dimeric interaction may aid in the selection of the reducing partner but likely does not interfere with heme binding. The heme iron is coordinated by a water molecule in the ferric form, but the distal water is absent in the ferrous form. In all of the Syn HO-2 structures, several water molecules form a hydrogen-bond network at the distal hemepocket, which is involved in HO activity. Upon NO binding, the side-chain conformation of Tyr 156 changes. Tyr 156 is located at the hydrophobic cluster, which interrupts the possible H^+ pathway from the molecular surface to the hemepocket. Thus, Tyr 156 may function as a H^+ shuttle by changing conformation.

Phytobilins are linear tetrapyrrole chromophores that are synthesized in plants, algae, and cyanobacteria. Phytobilins are covalently bonded to apoproteins and function as light sensors (phytochromobilins) (*2*) and light-harvesting pigments (phycobilins). The characteristic blue-green and red colors of cyanobacteria and red algae reflect the presence of light-harvesting complexes, called phycobilisomes, which are composed of proteins bound to phycobilins (*3*). Phycobilins are synthesized from heme; the porphyrin ring of heme is first cleaved by heme oxygenase (HO)[1] to produce biliverdin, and biliverdin is converted to phycobilins by one or two other enzymes (*4*).

HO has been characterized in mammalian systems as a membrane-bound microsomal enzyme that catalyzes the regiospecific oxidative degradation of heme (*5*). The enzymatic reaction catalyzed by HO requires several reduction equivalents, which are supplied from NADPH-cytochrome P450 reductase in mammalian systems and molecular oxygen (*6*−*8*). The inducible isoform of mammalian HO, HO-1, in complex with heme, has been characterized using solubilized recombinant proteins, in which the C-terminal segment that is anchored to the membrane was genetically removed (*9*, *10*). In the first step of the HO reaction, O_2 bound to the heme iron is activated to ferric hydroperoxide and electrophilic addition of the terminal oxygen to the α-*meso* carbon produces α-hydroxyheme. In the second step, α-hydroxyheme is converted to verdoheme with concomitant release of the α-*meso* carbon as CO. Finally, the oxygen bridge of verdoheme is cleaved to produce a biliverdin-iron chelate, and the iron is released prior to the dissociation of biliverdin (*6*−*8*). The reaction mechanism of the constitutively ex-

[†] This work was supported in part by Grants-in-Aid for Scientific Research (C) to K.F. (16570095) and T.Y. (14580641 and 16570108) and by a grant of the National Project on Protein Structural and Functional Analyses from the Ministry of Education, Culture, Sports, Science, and Technology of Japan.

[‡] Coordinates and structure factors have been deposited in the Protein Data Bank, accession codes 1WOV (ferric heme-Syn HO-2), 1WOW (ferrous heme-Syn HO-2), and 1WOX (NO-heme-Syn HO-2).

* To whom correspondence should be addressed. Telephone: +81-6-6850-5422. Fax: +81-6-6850-5425. E-mail: fukuyama@bio.sci.osaka-u.ac.jp.

[§] Osaka University.

[||] Yamagata University School of Medicine.

[⊥] Yamaguchi University.

[1] Abbreviations: Fd, ferredoxin; HO, heme oxygenase; HmuO, heme oxygenase from *Corynebacterium diphtheriae*; Syn HO-1, heme oxygenase-1 from *Synechocystis* sp. PCC 6803; Syn HO-2, heme oxygenase-2 from *Synechocystis* sp. PCC 6803; heme-Syn HO-1, Syn HO-1 in complex with heme; heme-Syn HO-2, Syn HO-2 in complex with heme; NO-heme-Syn HO-2, NO bound heme-Syn HO-2.

10.1021/bi0480483 CCC: $30.25
Published on Web 02/22/2005

pressed isoform of HO, HO-2, which contains an additional N-terminal segment, is similar to that of HO-1 (*11*). The crystal structures of the human (*12*) and rat HO-1s (*13*) in complex with heme and bacterial HOs [from the Gram-negative and Gram-positive pathogens, *Neisseria meningitidis* (*14*) and *Corynebacterium diphtheriae* (*15*)] in complex with heme have demonstrated that all of these HOs consist mostly of α helices with similar folding.

Although physiological functions, biochemical characteristics, and crystal structures of heme oxygenases (HOs) from mammals and pathogenic bacteria have been extensively studied, those of photosynthetic organisms are minimally studied. Two paralogs of *ho* (*ho1*, ORF sll1184, and *ho2*, ORF sll1875) are contained in the genome of *Synechocystis* sp. PCC 6803 (*16*). The *ho1* gene is expressed in *Synechocystis* sp. PCC 6803 and is induced by iron deficiency. Although the expression of *ho2* was not detected by Northern blotting analysis (*17*), the expression of this gene was detected by transcriptome analysis using a DNA microarray.[2] Both recombinant proteins [Syn HO-1 (*17, 18*) and Syn HO-2 (*19*)] possess *in vitro* heme degradation activity. Each amino acid sequence of Syn HO-1 and Syn HO-2 is equally similar to the sequences of mammalian HO-1 and HO-2; the identities of amino acid residues are 45% between Syn HO-1 and human HO-1, 50% between Syn HO-1 and human HO-2, 40% between Syn HO-2 and human HO-1, and 38% between Syn HO-2 and human HO-2. Both Syn HOs, as mammalian HO-1, do not have a N-terminal sequence motif conserved in mammalian HO-2 (*11*).

We have recently determined the crystal structure of Syn HO-1 in complex with heme and have demonstrated that Syn HO-1 shares a common folding with other HOs (*20*). We have now determined the crystal structure of Syn HO-2 in complex with heme, showing that the complex exists in a dimer form. We have also determined the structures of the reduced and NO-bound forms of this complex. Here, we present the characteristics of these structures and discuss the reaction mechanism.

EXPERIMENTAL PROCEDURES

Sample Preparation. Heme-Syn HO-1 was prepared as described (*18*). Apo-Syn HO-2 and heme-Syn HO-2 were prepared by similar methods (*19*). Briefly, recombinant *ho2* from *Synechocystis* sp. PCC 6803 was inserted into the T7-promoter-based expression vector, pMW172. The resulting expression plasmid was transformed into *Escherichia coli* BL21 (DE3) cells. Apo-Syn HO-2 protein was purified from the supernatant fraction of the cell lysate by ammonium sulfate fractionation and anion-exchange, hydroxyapatite, and gel-filtration chromatography steps. Heme-Syn HO-2 was prepared by the addition of a 1.2 equiv excess of hemin to apo-Syn HO-2 and purified with desalting and hydroxyapatite columns.

Characterization of the Molecular Assembly of Heme-Syn HO-2. The molecular assembly of apo-Syn HO-2, heme-Syn HO-2, and heme-Syn HO-1 was characterized by gel-filtration chromatography at 4 °C. Gel-filtration chromatography was performed using the ÄKTA explorer system (Amersham Biosciences) and a HiPrep 16/60 Sephacryl S-200 HR column (*2*) (Amersham Biosciences). Buffer containing 50 mM Tris-HCl (pH 7.4) and 50 mM NaCl was used for equilibration of the column and eluent. The flow rate was 0.4 mL/min for equilibration and elution. Blue dextran (2000 kD), alcohol dehydrogenase (150 kD), bovine serum albumin (66 kD), carbonic anhydrase (29 kD), and cytochrome *c* (12.4 kD) were contained in a molecular weight marker kit for gel-filtration chromatography (Sigma) that was used to estimate the molecular weight.

Crystallization of the Ferric Heme-Syn HO-2 Complex and Preparation of the Ferrous Complex and NO-Bound Form. Crystallization conditions for ferric heme-Syn HO-2 were screened with the Crystal Screen kit (Hampton Research) using the hanging-drop vapor-diffusion method. The protein solution was mixed with an equal volume of each reservoir solution and equilibrated. Crystals of ferric heme-Syn HO-2 were obtained at 293 K using a reservoir solution containing 0.2 M potassium sodium tartrate. The protein concentration for crystallization was 20 mg/mL in 0.1 M potassium phosphate buffer (pH 7.0). Plate-shaped crystals appeared after 1 day (Figure 1a). Ferric heme-Syn HO-2 crystals were dialyzed for 12 h with a crystallization solution containing 40% (w/v) sucrose as a cryoprotectant and were then flash-cooled under a nitrogen gas stream at 100 K.

Ferrous heme-Syn HO-2 crystals were prepared by soaking ferric heme-HO crystals for 5 min in a degassed solution containing an excess amount of sodium dithionite and 40% (w/v) sucrose. NO-heme-Syn HO-2 crystals were prepared by soaking ferrous heme-HO crystals for 5 min in a solution containing NOC-12, an autocatalytic NO donor (Dojindo, Kumamoto, Japan), an excess amount of sodium dithionite, and 40% (w/v) sucrose. Ferrous heme-Syn HO-2 and NO-heme-Syn HO-2 crystals on cryoloops were immediately cooled by liquid nitrogen and stored in liquid nitrogen until data collection.

Data Collection and Processing. Diffraction data for ferric heme-Syn HO-2 were collected at 100 K using synchrotron radiation ($\lambda = 1.063$ Å) at the BL41XU beamline at SPring-8 and a marCCD detector. The distance between the crystal and CCD was 110 mm. The crystal was oscillated by 1.0° per frame over a total measurement angle of 180°. Diffraction data for ferrous heme-Syn HO-2 and NO-heme-Syn HO-2 were collected in a similar manner using a 1.046 Å wavelength X-ray. All Diffraction data were processed, merged, and scaled using MOSFLM (*21*) and SCALA in a CCP4 package (*22*, *23*). Crystallographic data and diffraction statistics are given in Table 1a.

Determination of Twinned Properties and Separation of the Twinned Data into Individual Components. Although the ferric heme-Syn HO-2 crystal appeared to be a single crystal (Figure 1a), it was a nonmerohedral twin as characterized by the diffraction image analysis. The diffraction spots from this crystal were partially predictable; however, excess diffraction spots were observed when the crystal was assumed to be a single crystal (Figure 1b). When two crystal orientations, which are related by the 2-fold axis being vertical to the *ab* plane, were assumed to be present in this crystal, the observed diffraction spots appeared as predicted. Most of the diffraction spots could be predicted by assuming that the length of the *a* axis was doubled ($a = 116$ Å), but

[2] Expression data from DNA microarray analysis are published in the Kyoto Encyclopedia of Genes and Genomes database (*1*).

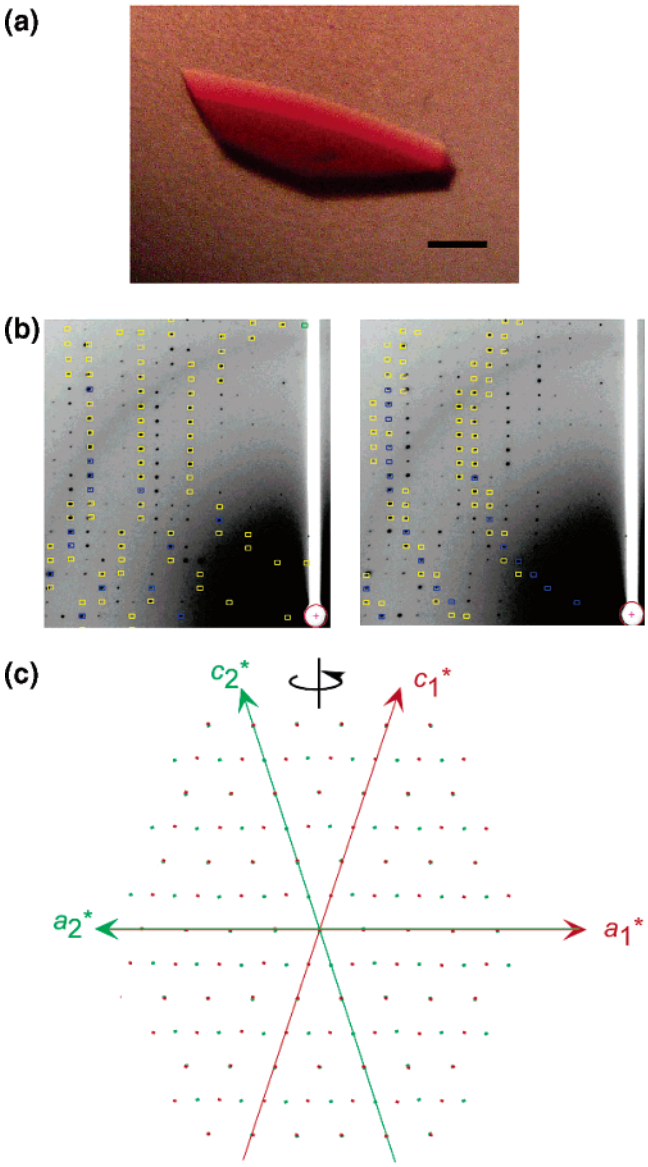

FIGURE 1: Analysis of the nonmerohedrally twinned crystal. (a) Heme-Syn HO-2 crystal. Scale bar indicates 0.1 mm. (b) Diffraction images of the heme-Syn HO-2 crystal. Predictions (yellow and blue squares) are superimposed. Predictions shown on the left and right sides are two possible indexing schemes. The two schemes are required for predicting all of the diffraction spots. (c) Reciprocal space of the nonmerohedrally twinned crystal. Red and green spots indicate the reciprocal lattice of each twin component. Diffractions of the twin components appear alternately with $l = 2n + 1$, whereas those with $l = 2n$ completely overlap.

initial phasing by the molecular replacement method was unsuccessful. Initial phasing by molecular replacement and further refinement assuming that the crystal was a nonmerohedral twin was successful. The crystal lattices of ferric heme-Syn HO-2 and ferrous heme-Syn HO-2 satisfied the condition $4a \cos \beta + c = 0$, indicating that the reciprocal space of each crystal is as shown in Figure 1c (*24*); the diffraction spots of each component with $l = 2n + 1$ alternately appeared as if the apparent crystal lattice, a, was doubled. The diffraction spots on every second line with $l = 2n$ overlapped with those of the other component, and it is necessary to obtain the true intensities (I_{true}) from the overlapped diffraction intensities. $I_{true}(h,k,l)$ can be derived from the following formulas (*25*).

$$I_{obs}(h,k,l) = (1 - \alpha)I_{true}(h,k,l) + \alpha I_{true}(h + l/2,-k,-l)$$

$$I_{obs}(h + l/2,-k,-l) = \alpha I_{true}(h,k,l) + (1 - \alpha)I_{true}(h + l/2,-k,-l)$$

Thus,

$$I_{true}(h,k,l) = \{(1 - \alpha)I_{obs}(h,k,l) - \alpha I_{obs}(h + l/2,-k,-l)\}/(1 - 2\alpha)$$

where α is the twinning fraction and I_{obs} is the apparently observed diffraction intensity. The twinning fractions were determined to be 0.18 for ferric heme-Syn HO-2 and 0.37 for ferrous heme-Syn HO-2 by comparison of two diffraction intensities with $l = 2n + 1$ from each twinning domain. The structure factors calculated from I_{true} were used for further structure refinement. The crystal lattice of NO-heme-Syn HO-2 did not satisfy the condition $4a \cos \beta + c = 0$; the diffraction spots of each twinning fraction did not overlap exactly. Therefore, observed structure factors were used for the refinement of the NO-heme-Syn HO-2 structure.

Model Building and Refinement. The structure of ferric heme-Syn HO-2 was determined by the molecular replacement method using MOLREP (*23*, *26*), in which the protein moiety of the heme-rat HO-1 complex (PDB code 1DVE) was used as the search model. A cross-rotation and translation search located two Syn HO-2 molecules in an asymmetric unit. After rigid-body refinement for the two polypeptide chains, these chains were substituted with the Syn HO-2 chain on the basis of the known sequence using the GeneMine homology modeling software (*27*). Simulated annealing and temperature-factor refinements were applied to the Syn HO-2 models based on 20.0−2.4 Å resolution data. The R factor was reduced to about 40% in this step. The heme and additionally ordered C-terminal helices and loops were clearly seen in the electron-density map and were included in the subsequent refinements. Using 20.0−2.0 Å resolution data, energy minimization and temperature-factor refinements were applied to the model and the R factor was reduced to about 25%. Refinements in these steps were performed using CNS (*28*). Water molecules were automatically picked up according to the criteria given by CNS (*28*); peaks above 3σ in the $F_o - F_c$ map located within a distance range of 2.0−4.0 Å from the model were assigned as water molecules. These were incorporated in the model together with a few isolated waters manually picked up. After the refinement, water molecules with a real space correlation less than 0.5 were deleted from the model by CNS (*28*). After a few cycles of water picking, energy minimization refinement, and manual adjustments of the model using XFIT (*29*), a final energy minimization refinement using 20.0−1.75 Å resolution data was performed using REFMAC5 (*30*) to incorporate alternate conformations of some residues.

The initial phases of ferrous heme-Syn HO-2 and NO-heme-Syn HO-2 were determined by the molecular-replacement method using the ferric heme-Syn HO-2 model as a searching model. Model refinements for ferrous heme-Syn HO-2 and NO-heme-Syn HO-2, including manual adjustments of the models and adding water, heme, and NO molecules, were performed as in the case of ferric heme-Syn HO-2, and final refinements of both models were

Table 1: Summary of Crystallographic Statistics

a. Crystallographic Statistics

crystallographic data	ferric heme-Syn HO-2		ferrous heme-Syn HO-2		NO-heme-Syn HO-2
space group	$P2_1$		$P2_1$		$P2_1$
unit cell dimensions (Å, deg)	$a = 58.16$, $b = 74.59$, $c = 72.66$, $\beta = 108.15$		$a = 58.03$, $b = 74.28$, $c = 72.27$, $\beta = 108.03$		$a = 57.31$ $b = 73.76$, $c = 71.07$, $\beta = 106.91$
number of molecules in an asymmetric unit	2		2		2
diffraction statistics	twinning fraction 1 (82%)	twinning fraction 2 (18%)	twinning fraction 1 (63%)	twinning fraction 2 (37%)	
resolution range (Å)	50−1.75	50−1.75	50−2.20	50−2.20	50−2.10
number of observations	201 910	202 989	102 214	102 242	134 243
number of unique reflections	54 377	55 189	29 770	30 108	33 226
redundancy	3.7	3.7	3.4	3.4	4.0
completeness (%)[a]	92.4 (94.9)	92.6 (95.0)	98.9 (98.6)	98.9 (98.9)	100.0 (100.0)
mean I_o/σ	5.5 (3.1)	4.7 (2.9)	5.4 (2.0)	5.8 (1.9)	5.3 (2.3)
R_{sym}[a,b]	0.076 (0.198)	0.084 (0.234)	0.103 (0.339)	0.102 (0.353)	0.110 (0.312)

b. Refinement Statistics

refinement statistics	ferric heme-Syn HO-2	ferrous heme-Syn HO-2	NO-heme-Syn HO-2
resolution range (Å)	20.0−1.75	20.0−2.20	20.0−2.10
R/R_{free}[c]	0.195/0.251	0.219/0.282	0.211/0.246
number of water molecules	642	469	311
rms deviations from ideality			
bond lengths (Å)	0.024	0.006	0.006
angles (deg)	1.97	1.14	1.18
Ramachandran plot			
most favored (%)	95.3	94.7	94.9
additionally allowed (%)	4.2	5.1	4.4
generously allowed (%)	0.5	0.2	0.7

[a] Values in parentheses are for the outermost shells (1.84−1.75 Å for ferric heme-Syn HO-2, 2.32−2.20 Å for ferrous heme-Syn HO-2, and 2.21−2.10 Å for NO-heme-Syn HO-2). [b] $R_{sym} = \sum_{hkl}\sum_i |I_i(hkl) - \langle I(hkl)\rangle|/\sum_{hkl}\sum_i I_i(hkl)$, where $\langle I(hkl)\rangle$ is the mean intensity for multiple recorded reflections. [c] $R = \sum|F_{obs}(hkl) - F_{calc}(hkl)|/\sum|F_{obs}(hkl)|$. R_{free} is the R value calculated for 5% of the dataset not included in the refinement.

performed with CNS (*28*). The geometry of the coordination of the heme iron was not restrained at the final stage of refinement. A stereochemical check of the model was made with PROCHECK (*31*). Interactions at the dimer interface were analyzed using the Protein−Protein Interaction Server (*32*). Final refinement statistics are given in Table 1b.

RESULTS

Dimeric Structure of Heme-Syn HO-2. The structures of two molecules (A and B) of ferric heme-Syn HO-2 in an asymmetric unit have been refined using 1.75 Å resolution data to an R factor of 0.195 and an R_{free} factor of 0.251 (Figure 2). The N-terminal Met residues in both molecules, the Ala 236−Ala 240 residues in molecule A, and the Ala 236−His 242 residues in molecule B were disordered. The structures of the two ferric heme-Syn HO-2 molecules consist mainly of α helices and are very similar to each other [(root-mean-square) rms deviation of Cα atoms is 0.25 Å]. The overall structure of the segment from helix A to helix H is similar to the structures of other HOs, including the kinked distal helix (F helix) and heme-binding site. One of the characteristic features of the ferric heme-Syn HO-2 structure is in the C-terminal ordered segment (Glu 210−Glu 250), which turns back near the hemepocket. The C-terminal segment consists of the I and J helices, a loop extended to the hemepocket, a disordered loop, and a β strand that interacts with the other molecule (Figure 2a). The two molecules are related by noncrystallographic 2-fold symmetry and interacted mainly through this segment (Figure 3a). The area of the dimer interface (1466 Å^2 per monomer), interactions between the two molecules [4 salt bridges and 18 hydrogen bonds, including 5 hydrogen bonds via water molecules (Table 2)], and complementarity between the two surfaces (gap volume index is 1.22) are consistent with the features of general homodimeric interactions (*32*). Gel-filtration analysis indicated that ferric heme-Syn HO-2 forms a homodimer, whereas ferric heme-Syn HO-1 forms a monomer. Interestingly, the majority of apo-Syn HO-2 exists as a monomer in solution (Figure 3b). It is noteworthy that Syn HO-2 forms a dimer upon heme binding and heme-Syn HO-2 is the first dimeric heme-HO.

The structures of ferrous heme-Syn HO-2 and NO-heme-HO-2 have been refined to R factors of 0.219 and 0.211 and R_{free} factors of 0.282 and 0.246, respectively (Figure 4). The structures of the ferrous heme-Syn HO-2 and NO-heme-Syn HO-2 subunits resemble the structure of the ferric heme-Syn HO-2 subunit. The dimeric interaction was unchanged following reduction, although the subunit was slightly twisted at the hydrogen bond between His 220 and Glu 34 upon NO binding.

Hemepocket Structure. As in other ferric heme-HOs, His 16 and a water molecule are coordinated to the heme iron

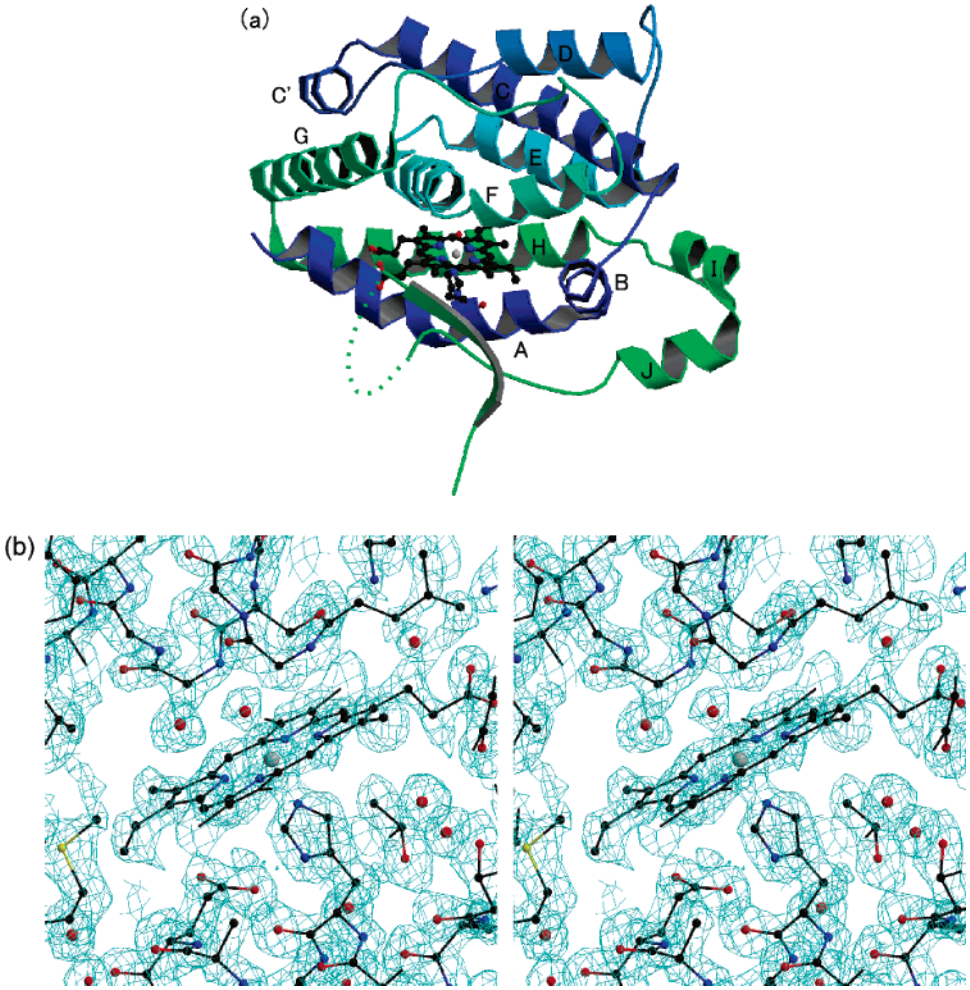

FIGURE 2: Crystal structure of heme-Syn HO-2. (a) Ribbon diagram of heme-Syn HO-2 monomer. In comparison with other HOs, a helix (C′) is inserted between the C and D helices and the C-terminal segment is ordered (I and J helices and β strand). Heme and its ligands are shown as ball-and-stick models. (b) Stereo diagram of electron density (contoured at 1.3σ) was superimposed on the model of ferric heme-Syn HO-2. The structure around the heme in subunit A is shown.

Table 2: Bond Lengths Involved in the Interactions in the Dimer Interface of Ferric Heme-Syn HO-2

a. salt bridges		A···B	B···A
Arg 167 NH2	Glu 250 OE1	2.61	2.86
Arg 167 NE	Glu 250 OE2	2.89	2.93
b. direct hydrogen bonds		**A···B**	**B···A**
Lys 30 O	Lys 30 NZ	2.96	3.01
Glu 34 OE1	His 220 NE	2.68	2.58
Ser 143 O	Arg 227 NH1	2.99	3.01
His 242 N	Gly 249 O	2.94	
Ile 244 N	Met 247 O	3.01	3.13
Ile 244 O	Met 247 N	3.42	3.47
Ile 244 O	Ile 246 N	2.83	2.75
c. indirect hydrogen bonds (via water molecule)		**A···B[a]**	**B···A[a]**
Gly 31 O	Leu 224 O	2.79	2.76
		2.83	2.85
Ile 217 O	Ile 217 O	2.73	
		2.49	
Ile 217 O	Thr 221 OG	2.73	2.49
		2.93	2.71

[a] Upper and lower numerals indicate the distances toward the water molecule.

on the proximal and distal sides, respectively, in ferric heme-Syn HO-2. The respective distances from the proximal and distal ligands to the heme iron were 2.0 and 2.1 Å in subunit A and 2.0 and 1.9 Å in subunit B. The carbonyl group of Gly 129 and the amide group of Gly 133 are able to hydrogen-bond to the distal water, as in rat heme-HO (the two glycine residues correspond to Gly 139 and Gly 143 in rat HO-1, respectively) (*13*). The orientation of heme binding is stabilized by electrostatic interactions and hydrogen bonds between the propionate groups of heme and Arg 9, Tyr 124, Lys 171, and Arg 175. On the distal side of heme-Syn HO-2, water molecules form a hydrogen-bond network that includes Arg 126 and Asp 130 (which correspond to Arg 136 and Asp 140 in mammalian HO-1, respectively). This hydrogen-bond network and distal aspartic acid have been proposed to be involved in H^+ transfer to and activation of the distal dioxygen in mammalian HO-1 (*33*, *34*). This conserved hydrogen-bond network and Asp 130 likely functions in Syn HO-2 as proposed in mammalian HO-1. In contrast to the hydrogen-bond network seen in mammalian HO-1, the hydroxyl group of Tyr 156 is hydrogen-bonded to this network as is the case in Syn HO-1 (*20*) and in HO from *Corynebacterium diphtheriae* (HmuO) (*15*). Tyr 156 is also conserved in HOs of higher-plants, algae, and mammalian HO-2 but is substituted by Phe in mammalian HO-1. One of the characteristic features of Syn HO-2 is on the proximal side of the heme. As in other HOs, the Nδ atom of the proximal histidine is able to hydrogen-bond to

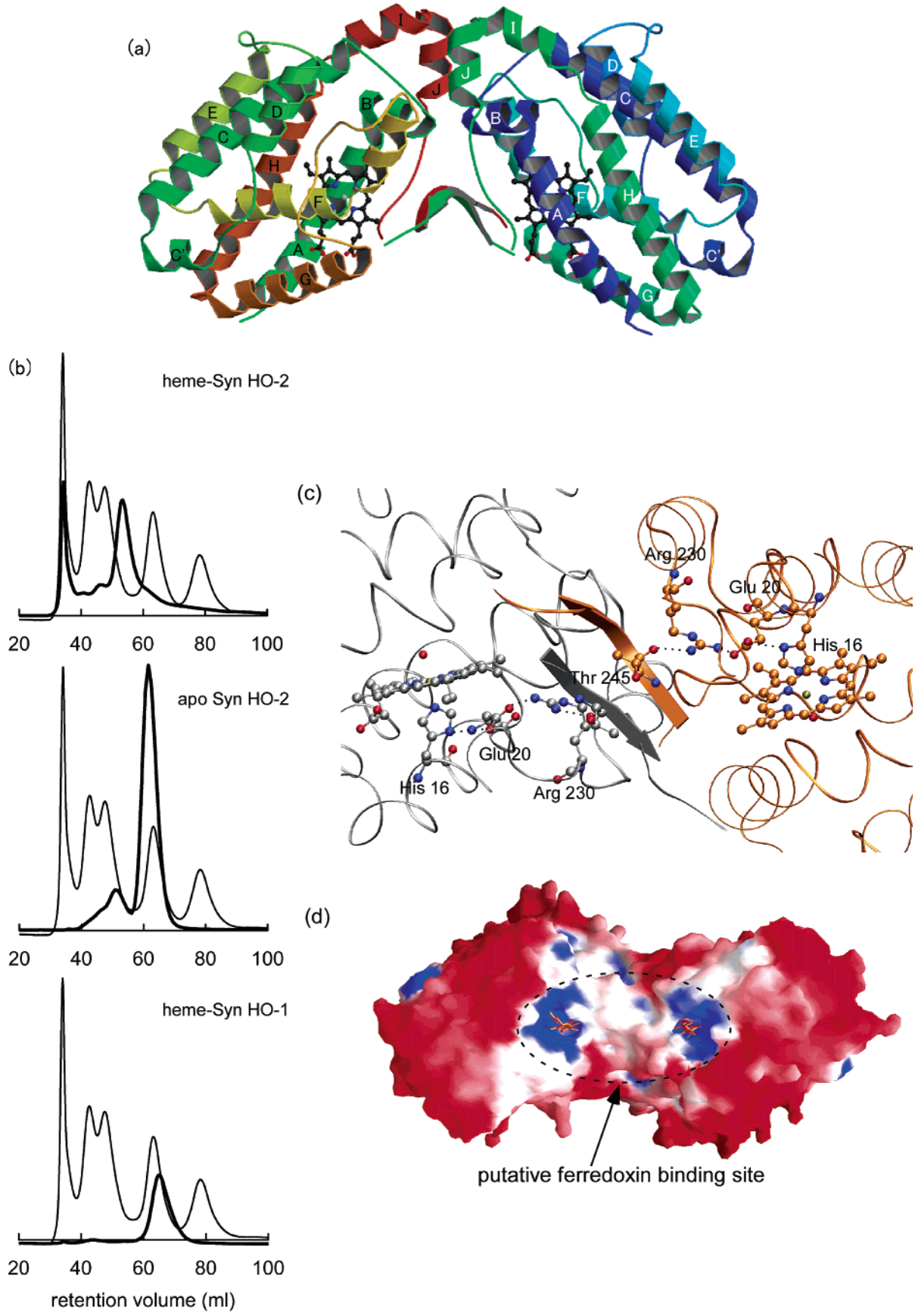

FIGURE 3: Dimeric structure of heme-Syn HO-2. (a) Ribbon diagram of the heme-Syn HO-2 dimer. (b) Gel-filtration chromatograms of heme-Syn HO-2 (upper), apo-Syn HO-2 (middle), heme Syn HO-1 (lower) are shown. All of these are superimposed on a molecular marker (thin line). The vertical and horizontal axes show absorbance at 280 nm and the retention volume, respectively. The molecular weights of Syn HO-1 and Syn HO-2 estimated from their amino acid sequences are 27.1 and 28.5 kD, respectively. (c) Proximal hydrogen-bond network (subunit A, orange; subunit B, gray). (d) Molecular surface of dimeric heme-Syn HO-2 colored by electrostatic potential (blue, basic; red, acidic) is superimposed on the ball-and-stick model of heme.

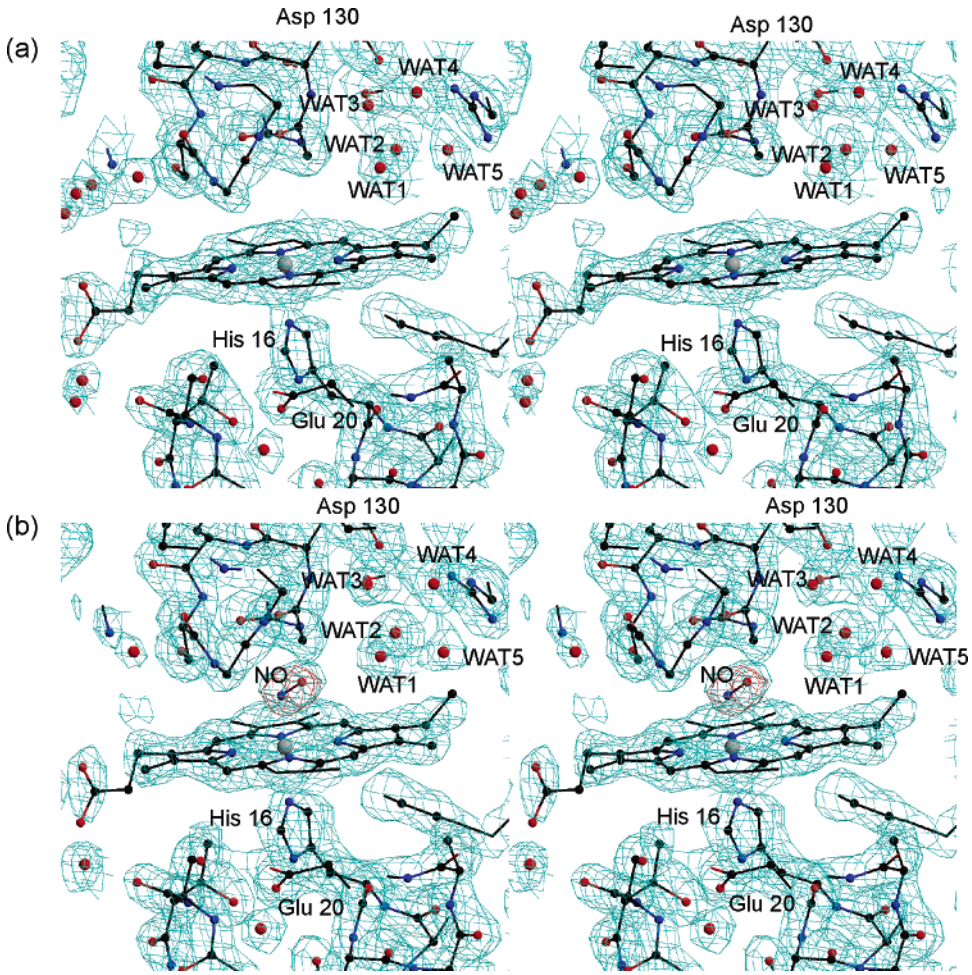

FIGURE 4: Structures around the heme molecule in ferrous heme-Syn HO-2 and NO-heme-Syn HO-2. Stereo diagrams of electron density (cyan, contoured at 1.3σ) were superimposed on the ball-and-stick models of ferrous heme-Syn HO-2 (a) and NO-heme-Syn HO-2 (b). A σ_A weighted $F_o - F_c$ map with the NO bound to the heme iron (red, contoured at 5.0σ) omitted is superimposed on the model.

the carboxyl group of Glu 20. In addition, the carboxyl group of Glu 20 is able to hydrogen-bond to Arg 230, which is also hydrogen-bonded to the carbonyl group of Thr 245 (Figure 3c). These bonds constitute one of the factors ordering the C-terminal segment.

Upon reduction of the heme iron, the distal water molecule disappeared. NO bound to the ferrous heme iron was clearly seen in the electron-density map (Figure 4). The NO molecule was highly bent toward the α-*meso* edge of the heme. The Fe···N−O angle converged to 125° in subunit A and 118° in subunit B, and the Fe···N length converged to 2.1 Å in both subunits by the refinement. The distances between the oxygen atom of the NO molecule and the α-*meso* edge of the heme were 3.5 Å in subunit A and 3.6 Å in subunit B. The distal hydrogen-bond network in ferric heme-Syn HO-2 was also conserved in ferrous heme-Syn HO-2 and NO-heme-Syn HO-2. One of the water molecules in the distal hydrogen-bond network and the amide group of Gly 133 is able to hydrogen-bond to the oxygen and nitrogen atoms of the NO molecule, respectively. The respective distances from the NO molecule to this water molecule and the amide nitrogen of Gly 133 were 3.2 and 2.9 Å in subunit A and 3.0 and 2.9 Å in subunit B. The NO-binding geometry was very similar to that seen in rat heme-HO-1 (*35*), although heme-Syn HO-2 forms a homodimer and the C-terminal segment directly interacts with the proximal and distal helices. The structural change upon reduction of the heme iron and NO binding was very small, except for the χ1 angle of Tyr 156 (Figure 5); the hydroxyl oxygen of Tyr 156 moves by 0.9 Å toward the hemepocket upon NO binding.

DISCUSSION

Possible Functional Differences between Monomeric and Dimeric HOs. On the basis of the molecular packing in the crystal and the results of gel-filtration chromatography, we first determined that the oligomeric state of Syn HO-2 changes upon heme binding. The dimer interface is mostly composed of the C-terminal segment (the I and J helices and β strand). Arg 230 in the loop between the J helix and β strand is salt-bridged to Glu 20, which is hydrogen-bonded to the proximal ligand, His 16 (Figure 3c). This interaction serves to stabilize the position of the loop between the J helix and β strand. Releasing the heme from heme-Syn HO-2 may cause drastic conformational changes in the heme pocket. It is likely that fluctuation of the proximal ligand, His 16, will increase when the heme is removed; this would cause a conformational change in the proximal helix. Indeed, the proximal helix is disordered in apo-rat HO-1 (*36*). In apo-human HO-1, the position of the proximal histidine moves away from the heme pocket (*37*). The conformational change of the proximal helix in Syn HO-2 may lead to the loss of the interaction among His 16, Glu 20, and Arg 230; this may

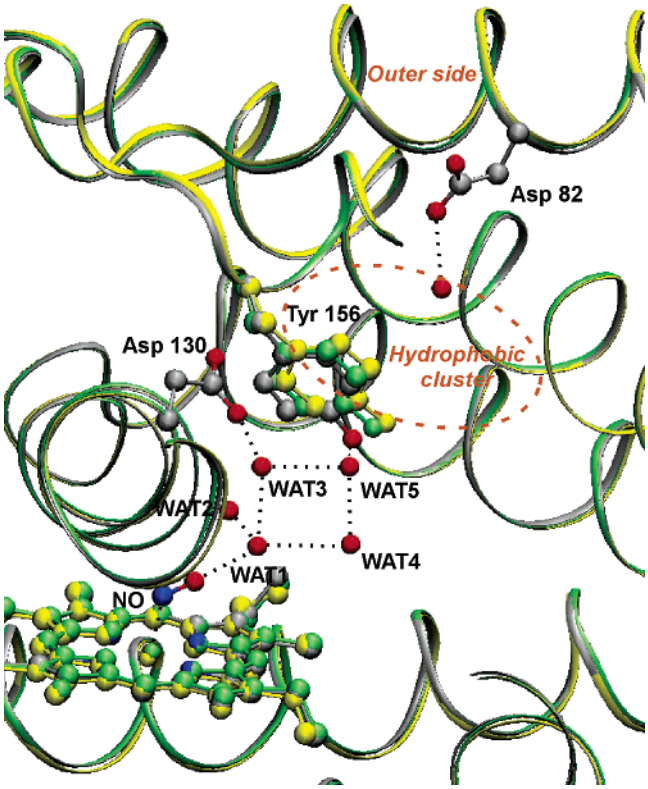

FIGURE 5: Possible hydrogen-bond network from the molecular surface to the hemepocket. Ribbon diagrams of ferric heme-Syn HO-2 (yellow), ferrous heme-Syn HO-2 (lime green), and NO-heme-Syn HO-2 (gray) are superimposed. Hemes, NO, water molecules, and amino acid residues involved in the distal hydrogen-bond network are shown as ball-and-stick models. The three Syn HO-2 models were superimposed by minimizing the rms deviations of Cα atoms of one subunit. The hydrophobic cluster separates the hydrogen-bond network from the outer side of the molecule to the hemepocket.

cause fluctuation of the C-terminal segment and result in a change of the oligomeric state of Syn HO-2 from dimer to monomer.

The dimeric interaction partially covers the surface of the heme-binding side and may affect the accessibility of heme, although part of the heme is exposed to the molecular surface in the heme-Syn HO-2 dimer (Figure 3d). The change in the oligomeric state upon heme binding may serve to maintain smooth substrate binding and product release as in monomeric HO.

Reducing equivalents and molecular oxygen are required for the HO reaction. Dimerization of Syn HO-2 would also affect the molecular interactions with its reducing partner. [2Fe-2S] ferredoxin (Fd) has been proposed as a physiological electron donor for Syn HO-1 (*17*, *38*), whereas the donor for Syn HO-2 is unknown, although Fd can serve reducing equivalents to Syn HO-2 *in vitro* (*19*). On the basis of the electrostatic potential of the molecular surface and molecular interaction analysis of HO using the fluorescent energy transfer technique (*39*), mammalian HO-1 interacts with the reduction enzyme (NADPH-cytochrome P450 reductase) on the heme-binding side. Syn HO-1 may also interact with Fd at the basic patch on the heme-binding side, although the basic patch is narrower than that in mammalian HO-1 and is suited for interaction with a small reducing protein (*20*). The heme-binding side of heme-Syn HO-2 is partially covered by the second subunit, leaving only enough space for one molecule of a small acidic protein such as Fd to bind in the groove of the heme-Syn HO-2 dimer (Figure 3d). Such a difference in the putative Fd-binding sites of Syn HO-1 and Syn HO-2 was expected to affect the reduction rate using Fd, but biochemical analysis of Syn HO-1 and Syn HO-2 indicated that any significant difference between Syn HO-1 and Syn HO-2 was not so far observed in the HO activity. The activity of Syn HO-2 is comparable to that of Syn HO-1 *in vitro* using spinach Fd as a reductant (*19*). In conclusion, dimerization of Syn HO-2 apparently affects neither the efficiency of heme iron reduction nor heme-binding speed.

Although it is clearly shown that the molecular surface and shape are markedly changed upon dimerization and hence such change would alter the molecular recognition of Syn HO-1 and Syn HO-2, physiological significances of dimerization of Syn HO-2 are still unclear. Genome analysis (*16*) shows that four paralogs of [2Fe-2S] Fd (CyanoBase accession numbers sll0020, slr0150, sll1382, and slr1828), which differ in the expression pattern and physiological role, are present in *Synecocystis* sp. PCC 6803. Different molecular recognition of Syn HO-1 and Syn HO-2 would be related to the selection of four paralogs of Fd.

Extended Hydrogen-Bond Network and Possible H^+ Pathway from the Molecular Surface to the Hemepocket. As in the previously reported monomeric HO structures, several water molecules in the distal hemepocket form a hydrogen-bond network in dimeric heme-Syn HO-2. NO bound to the heme iron is hydrogen-bonded to a water molecule in this hydrogen-bond network. O_2 may bind to the heme iron in Syn HO-2 in a manner similar to NO binding. Indeed O_2 is bound to the heme iron in a similar manner as NO, including stabilization by water molecules and the amide group of glycine in HmuO (*40*). These indicate that the environment of the distal heme pocket of dimeric heme-Syn HO-2 is identical to that of other monomeric heme-HOs and that the O_2 activation mechanism is the same in dimeric and monomeric heme-HOs. On the basis of mutagenesis, crystal structures, and spectroscopic analyses, it has been proposed that this hydrogen-bond network is an H^+ pathway for O_2 activation in HOs (*33*−*35*, *40*−*44*). However, the H^+ pathway is discontinuous to the molecular surface in the crystal structure of mammalian HO-1 (*12*, *13*), although NMR analysis suggests that this pathway extends to the molecular surface (*44*). In HmuO, an extended pathway through Tyr 161 (Tyr 156 in Syn HO-2), Gln 46 (Leu 42 in Syn HO-2), and Asp 86 (Asp 82 in Syn HO-2) is suggested based on the crystal structure (*15*). Two hydrophobic residues (Phe and Met) in mammalian HO-1 are substituted with hydrophilic residues (Tyr and Gln) in HmuO. In Syn HO-2, Phe is substituted with Tyr and Tyr 156 interacts with the distal hydrogen-bond network as in HmuO. The Met residue is not substituted with a hydrophilic residue. Amino acid sequence alignment of the HOs from several species indicates that this hydrophilic substitution occurs only in mammalian HO-2 and HmuO and that residue 51 of mammalian HO-1 is conserved by hydrophobic residues in higher-plant, algae, and cyanobacterial HOs. The hydrogen-bond network from the hemepocket to the molecular surface proposed in HmuO (*15*) is interrupted by hydrophobic residues in Syn HO-2 and mammalian HO-1 (*12*, *13*).

It should be noted that this extended H^+ pathway may be continuous when a conformational change in the side chain of Tyr 156 occurs. The distance between the hydroxyl group of Tyr 156 and the water molecule hydrogen-bonded to the carboxyl group of Asp 82 changes upon the state of the heme iron; the distances are 5.3 Å in ferric heme-Syn HO-2, 5.5 Å in ferrous heme-Syn HO-2, and 6.2 Å in NO-heme-Syn HO-2 (Figure 5). These changes are achieved by changing the χ1 angle of Tyr 156. When the χ1 angle of Tyr 156 is changed about 30°, Tyr 156 is connected to the molecular surface via water molecule and Asp 82. This can be achieved without stereochemical collision, and thus, Tyr 156 may function as a H^+ shuttle between the molecular surface and the distal hemepocket in response to the oxidation and ligation status of the protein.

ACKNOWLEDGMENT

We thank Drs. Masahide Kawamoto and Hisanobu Sakai of JASRI for their aid with data collection using the synchrotron radiation at SPring-8.

REFERENCES

1. Kanehisa, M., Goto, S., Kawashima, S., and Nakaya, A. (2002) The KEGG databases at GenomeNet, *Nucleic Acids Res. 30*, 42−46.
2. Schafer, E., and Bowle, C. (2002) Phytochrome-mediated photoperception and signal transduction in higher plants, *EMBO Rep. 3*, 1042−1048.
3. Grossman, A. R., Schaefer, M. R., Chiang, G. G., and Collier, J. L. (1993) The phycobilisome, a light-harvesting complex responsive to environmental conditions, *Microbiol. Rev. 57*, 725−749.
4. Tooley, A. J., Cai, Y. A., and Glazer, A. N. (2001) Biosynthesis of a fluorescent cyanobacterial C-phycocyanin holo-α subunit in a heterologous host, *Proc. Natl. Acad. Sci. U.S.A. 98*, 10560−10565.
5. Tenhunen, R., Marver, H. S., and Schmid, R. (1968) The enzymatic conversion of heme to bilirubin by microsomal heme oxygenase, *Proc. Natl. Acad. Sci. U.S.A. 61*, 748−755.
6. Sono, M., Roach, M. P., Coulter, E. D., and Dawson, J. H. (1996) Heme-containing oxygenases, *Chem. Rev. 96*, 2841−2888.
7. Ortiz de Montellano, P. R. (2000) The mechanism of heme oxygenase, *Curr. Opin. Chem. Biol. 4*, 221−227.
8. Yoshida, T., and Migita, C. T. (2000) Mechanism of heme degradation by heme oxygenase, *J. Inorg. Biochem. 82*, 33−41.
9. Ishikawa, K., Sato, M., Ito, M., and Yoshida, T. (1992) Importance of histidine residue 25 of rat heme oxygenase for its catalytic activity, *Biochem. Biophys. Res. Commun. 182*, 981−986.
10. Wilks, A., and Ortiz de Montellano, P. R. (1993) Rat liver heme oxygenase. High level expression of a truncated soluble form and nature of the meso-hydroxylating species, *J. Biol. Chem. 268*, 22357−22362.
11. Ishikawa, K., Takeuchi, N., Takahashi, S., Mansfield Matera, K., Sato, M., Shibahara, S., Rousseau, D. L., Ikeda-Saito, M., and Yoshida, T. (1995) Heme oxygenase-2. Properties of the heme complex of the purified tryptic fragment of recombinant human heme oxygenase-2, *J. Biol. Chem. 270*, 6345−6350.
12. Schuller, D. J., Wilks, A., Ortiz de Montellano, P. R., and Poulos, T. L. (1999) Crystal structure of human heme oxygenase-1, *Nat. Struct. Biol. 6*, 860−867.
13. Sugishima, M., Omata, Y., Kakuta, Y., Sakamoto, H., Noguchi, M., and Fukuyama, K. (2000) Crystal structure of rat heme oxygenase-1 in complex with heme, *FEBS Lett. 471*, 61−66.
14. Schuller, D. J., Zhu, W., Stojiljkovic, I., Wilks, A., and Poulos, T. L. (2001) Crystal structure of heme oxygenase from the Gram-negative pathogen *Neisseria meningitidis* and a comparison with mammalian heme oxygenase-1, *Biochemistry 40*, 11552−11558.
15. Hirotsu, S., Chu, G. C., Unno, M., Lee, D. S., Yoshida, T., Park, S. Y., Shiro, Y., and Ikeda-Saito, M. (2004) The crystal structures of the ferric and ferrous forms of the heme complex of Hmu O, a heme oxygenase of *Corynebacterium diphtheriae*, *J. Biol. Chem. 279*, 11937−11947.
16. Kaneko, T., Sato, S., Kotani, H., Tanaka, A., Asamizu, E., Nakamura, Y., Miyajima, N., Hirosawa, M., Sugiura, M., Sasamoto, S., Kimura, T., Hosouchi, T., Matsuno, A., Muraki, A., Nakazaki, N., Naruo, K., Okumura, S., Shimpo, S., Takeuchi, C., Wada, T., Watanabe, A., Yamada, M., Yasuda, M., and Tabata, S. (1996) Sequence analysis of the genome of the unicellular cyanobacterium *Synechocystis* sp. strain PCC6803. II: Sequence determination of the entire genome and assignment of potential protein-coding regions, *DNA Res. 3*, 109−136.
17. Cornejo, J., Willows, R. D., and Beale, S. I. (1998) Phytobilin biosynthesis: Cloning and expression of a gene encoding soluble ferredoxin-dependent heme oxygenase from *Synechocystis* sp. PCC 6803, *Plant J. 15*, 99−107.
18. Migita, C. T., Zhang, X., and Yoshida, T. (2003) Expression and characterization of cyanobacterium heme oxygenase, a key enzyme in the phycobilin synthesis: Properties of the heme complex of recombinant active enzyme, *Eur. J. Biochem. 270*, 687−698.
19. Zhang, X., Migita, C. T., Sato, M., Sasahara, M., and Yoshida, T. (2005) Protein expressed by the *ho2* gene of the cyanobacteirum *Synechocystis* sp. PCC 6803 is a true heme oxygenase: Properties of the heme and enzyme complex, *FEBS J. 272*, 1012−1022.
20. Sugishima, M., Migita, C. T., Zhang, X., Yoshida, T., and Fukuyama, K. (2004) Crystal structure of heme oxygenase-1 from cyanobacterium *Synechocystis* sp. PCC 6803 in complex with heme, *Eur. J. Biochem. 271*, 4517−4525.
21. Leslie, A. G. W. (1992) Recent changes to the MOSFLM package for processing film and image plate data, *Joint CCP4 and ESF-EAMCB Newsl. Protein Crystallogr., 26*.
22. Kabsch, W. (1988) Evaluation of single-crystal X-ray diffraction data from a position-sensitive detector, *J. Appl. Crystallogr. 21*, 916−924.
23. Collaborative Computational Project, Number 4 (1994) The CCP4 suite: programs for protein crystallography, *Acta Crystallogr., Sect. D 50*, 760−763.
24. Dauter, Z. (2003) Twinned crystals and anomalous phasing, *Acta Crystallogr., Sect. D 59*, 2004−2016.
25. Redinbo, M. R., and Yeates, T. O. (1993) Structure determination of plastocyanin from a specimen with a hemihedral twinning fraction of one-half, *Acta Crystallogr., Sect. D 49*, 375−380.
26. Vagin, A., and Teplyakov, A. (1997) MOLREP: An automated program for molecular replacement, *J. Appl. Crystallogr. 30*, 1022−1025.
27. Lee, C., and Irizarry, K. (2001) The GeneMine System for genome/proteome annotation and collaborative data mining, *IBM Syst. J. 40*, 592−603.
28. Brünger, A. T., Adams, P. D., Clore, G. M., DeLano, W. L., Gros, P., Grosse-Kunstleve, R. W., Jiang, J. S., Kuszewski, J., Nilges, M., Pannu, N. S., Read, R. J., Rice, L. M., Simonson, T., and Warren, G. L. (1998) Crystallography and NMR system: A new software suite for macromolecular structure determination, *Acta Crystallogr., Sect. D 54*, 905−921.
29. McRee, D. E. (1999) XtalView/Xfit—A versatile program for manipulating atomic coordinates and electron density, *J. Struct. Biol. 125*, 156−165.
30. Pannu, N. S., Murshudov, G. N., Dodson, E. J., and Read, R. J. (1998) Incorporation of prior phase information strengthens maximum-likelihood structure refinement, *Acta Crystallogr., Sect. D 54*, 1285−1294.
31. Laskowski, R. A., MacArthur, M. W., Moss, D. S., and Thornton, J. M. (1993) PROCHECK: A program to check the stereochemical quality of protein structures, *J. Appl. Crystallogr. 26*, 283−291.
32. Jones, S., and Thornton, J. M. (1996) Principles of protein−protein interactions, *Proc. Natl. Acad. Sci. U.S.A. 93*, 13−20.
33. Lightning, L. K., Huang, H., Moenne-Loccoz, P., Loehr, T. M., Schuller, D. J., Poulos, T. L., and Ortiz de Montellano, P. R. (2001) Disruption of an active site hydrogen bond converts human heme oxygenase-1 into a peroxidase, *J. Biol. Chem. 276*, 10612−10619.
34. Fujii, H., Zhang, X., Tomita, T., Ikeda-Saito, M., and Yoshida, T. (2001) A role for highly conserved carboxylate, aspartate-140, in oxygen activation and heme degradation by heme oxygenase-1, *J. Am. Chem. Soc. 123*, 6475−6484.
35. Sugishima, M., Sakamoto, H., Noguchi, M., and Fukuyama, K. (2003) Crystal structures of ferrous and CO-, CN^--, and NO-bound forms of rat heme oxygenase-1 (HO-1) in complex with heme: Structural implications for discrimination between CO and O_2 in HO-1, *Biochemistry 42*, 9898−9905.

36. Sugishima, M., Sakamoto, H., Kakuta, Y., Omata, Y., Hayashi, S., Noguchi, M., and Fukuyama, K. (2002) Crystal structure of rat apo-heme oxygenase-1 (HO-1): Mechanism of heme binding in HO-1 inferred from structural comparison of the apo and heme complex forms, *Biochemistry 41*, 7293−7300.
37. Lad, L., Schuller, D. J., Shimizu, H., Friedman, J., Li, H., Ortiz de Montellano, P. R., and Poulos, T. L. (2002) Comparison of the heme-free and -bound crystal structures of human heme oxygenase-1, *J. Biol. Chem. 278*, 7834−7843.
38. Cornejo, J., and Beale, S. I. (1997) Phycobilin biosynthetic reaction in extracts of cyanobacteria, *Photosynth. Res. 51*, 223−230.
39. Wang, J., and Ortiz de Montellano, P. R. (2003) The binding sites on human heme oxygenase-1 for cytochrome P450 reductase and biliverdin reductase, *J. Biol. Chem. 278*, 20069−20076.
40. Unno, M., Matsui, T., Chu, G. C., Couture, M., Yoshida, T., Rousseau, D. L., Olson, J. S., and Ikeda-Saito, M. (2004) Crystal structure of the dioxygen-bound heme oxygenase from *Corynebacterium diphtheriae*: Implications for heme oxygenase function, *J. Biol. Chem. 279*, 21055−21061.
41. Sugishima, M., Sakamoto, H., Higashimoto, Y., Omata, Y., Hayashi, S., Noguchi, M., and Fukuyama, K. (2002) Crystal structure of rat heme oxygenase-1 in complex with heme bound to azide: Implication for regiospecific hydroxylation of heme at the α-*meso* carbon, *J. Biol. Chem. 277*, 45086−45090.
42. Lad, L., Wang, J., Li, H., Friedman, J., Bhaskar, B., Ortiz de Montellano, P. R., and Poulos, T. L. (2003) Crystal structures of the ferric, ferrous, and ferrous-NO forms of the Asp140Ala mutant of human heme oxygenase-1: Catalytic implications, *J. Mol. Biol. 330*, 527−538.
43. Davydov, R., Kofman, V., Fujii, H., Yoshida, T., Ikeda-Saito, M., and Hoffman, B. M. (2002) Catalytic mechanism of heme oxygenase through EPR and ENDOR of cryoreduced oxy-heme oxygenase and its Asp 140 mutants, *J. Am. Chem. Soc. 124*, 1798−1808.
44. Li, Y., Syvitski, R. T., Auclair, K., Wilks, A., Ortiz de Montellano, P. R., and La Mar, G. N. (2002) Solution NMR characterization of an unusual distal H-bond network in the active site of the cyanide-inhibited, human heme oxygenase complex of the symmetric substrate, 2,4-dimethyldeuteriohemin, *J. Biol. Chem. 277*, 33018−33031.

BI0480483